Instrument for x-ray magnetic circular dichroism measurements at high pressures

D. Haskel,[a] Y. C. Tseng, and J. C. Lang
Magnetic Materials Group, Advanced Photon Source, Argonne National Laboratory, Argonne, lllinois 60439

S. Sinogeikin
HPCAT, Carnegie Institution of Washington, Advanced Photon Source, Argonne National Laboratory, Argonne, lllinois 60439

(Received 29 May 2007; accepted 30 July 2007; published online 23 August 2007)

An instrument has been developed for x-ray magnetic circular dichroism (XMCD) measurements at high pressures and low temperatures. This instrument couples a nonmagnetic copper-beryllium diamond anvil cell featuring perforated diamonds with a helium flow cryostat and an electromagnet. The applied pressure can be controlled *in situ* using a gas membrane and calibrated using Cu *K*-edge x-ray absorption fine structure measurements. The performance of this instrument was tested by measuring the XMCD spectra of the $Gd_5Si_2Ge_2$ giant magnetocaloric material. © *2007 American Institute of Physics.* [DOI: 10.1063/1.2773800]

I. INTRODUCTION

The relative alignment of electronic spins in neighboring sites of a solid is intimately connected with the overlap of their electronic orbitals through Pauli's exclusion principle. Altering this overlap by the application of pressure, for example, has profound effects on the magnetic interactions, whether the wave functions of spin-carrying electrons overlap directly (*direct exchange*),[1] or indirectly through their hybridization with electronic orbitals of nonmagnetic ions (*superexchange*),[2] or conduction electrons (*indirect exchange*).[3] When combined with the element and orbital specificity of x-ray magnetic circular dichroism (XMCD),[4] high-pressure studies of magnetism provide a unique tool for understanding magnetic interactions in complex systems.[5–7]

Unlike neutron- and high-energy x-ray scattering probes of condensed matter at high pressures, the resonant nature of x-ray magnetic circular dichroism (XMCD) requires tuning the x-ray energy to selected absorption edges.[4] While the $L_{2,3}$ absorption edges of transition metal (TM) atoms ($2p \rightarrow 3d$ transition) and $M_{4,5}$ absorption edges of rare-earth (RE) atoms ($3d \rightarrow 4f$ transition) are widely used due to the sizable dichroic effects arising from the large spin polarization of $3d$, $4f$ final states, the relatively low excitation energies in the range of 500–1500 eV are not compatible with the highly absorbing diamond windows of high-pressure cells. A 100-μm-thick diamond crystal, for example, attenuates such x-ray beams by more than 10^{12}. The relatively higher energies of TM *K* edges ($1s \rightarrow 4p$) and RE $L_{2,3}$ edges ($2p \rightarrow 5d$) in the range of 5000–9000 eV, on the other hand, are more suitable for diamond anvil cell (DAC) measurements. For example, a 1-mm-thick diamond crystal reduces the x-ray intensity by only approximately ten times at the Fe *K* edge (7.112 keV). The dichroic effects at these higher-energy resonances, however, are reduced since the polarization in the $4p$, $5d$ final states probed by these transitions is only a small fraction of that in $3d$, $4f$ states. In addition, the absence of spin-orbit interaction in the initial $1s$ state of *K*-edge absorption results in a low spin polarization of the excited photoelectron with the observed dichroism signal arising solely from the weak spin-orbit coupling in the excited $4p$ state. While XMCD signals at TM *K* and RE $L_{2,3}$ edges are weaker, in the 0.1%–6% range, they are routinely measured at a number of synchrotron radiation sources.[8–10]

In this article, we report on the development of a high-pressure XMCD capability in the hard x-ray regime ($\gtrsim$5 keV) for studies of element-specific magnetism at high pressures. The setup features a DAC with perforated diamond anvils to minimize x-ray absorption, coupled with a flow cryostat and electromagnet for in-field studies at low temperatures. The instrument described in this article improves upon previously reported high-pressure XMCD setups in several respects. This setup adds low-temperature capability, increased field strength and ability to change pressure *in situ* over the setup described in Ref. 5, and nearly doubles the maximum field strength and increases the signal-to-noise ratio by incorporating perforated diamond anvils relative to the setup described in Ref. 6. We discuss the challenges associated with these measurements. In addition, we test the instrument by carrying out measurements on technologically relevant $Gd_5Si_2Ge_2$ magnetocaloric materials,[11,12] where large enhancements in ferromagnetic ordering temperature occur under applied pressure.[13,14]

II. EXPERIMENT

A. General setup

The high-pressure XMCD setup, including polarizing and focusing x-ray optics, is shown in Fig. 1. A 1×1 mm^2 x-ray beam produced by a 2.4-m-long linear undulator insertion device ($\sim 5 \times 10^{12}$ photons/s) is monochromatized by a Si(111) fixed-exit double-crystal monochromator.[15] For the

[a]Electronic mail: haskel@aps.anl.gov

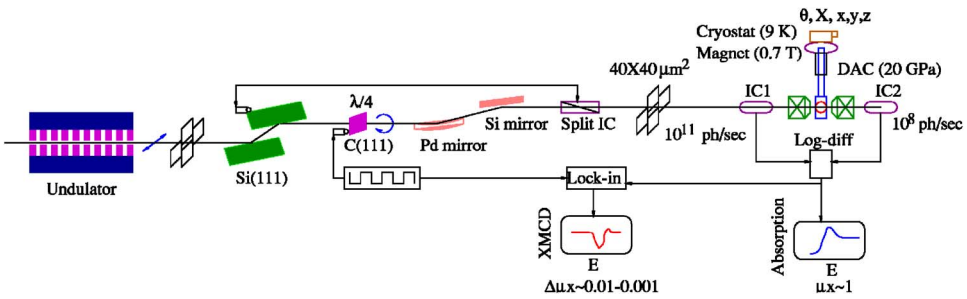

FIG. 1. (Color online) Experimental setup for high-pressure XMCD measurements.

XMCD measurements, the polarization of the undulator x-ray beam, which is linear in the plane of the synchrotron orbit, is converted to circular by means of a C(111), 100-μm-thick diamond crystal phase retarder (PR) optic operated in Bragg-transmission geometry.[16] The PR attenuates the beam intensity by approximately two times at the Fe *K* edge (7.112 keV). Toroidal (Pd) and flat (Si) mirrors at 5 mrad incidence angle focus the x-ray beam to $\sim 150 \times 250$ μm^2 at the position of the defining slit before the sample. The combined harmonic rejection of the two mirrors is $\sim 10^5$ at 7 keV. Additional harmonic rejection can be obtained by detuning of the second Si(111) crystal away from its Bragg condition. A high level of harmonic rejection is critically important for these measurements due to the significant attenuation of the fundamental x-ray beam in the phase retarder, diamond anvils, and sample ($\sim$100–500 times at 7 keV). A split ionization chamber is used to monitor and maintain a fixed vertical beam position by adjusting the angular position of the second Si(111) crystal. A feedback loop, which minimizes the difference in photoinduced current in the split chambers relative to a set value, is used for this purpose. The x-ray beam size is further reduced by a defining slit to $\sim 40 \times 40$ μm^2, which is smaller than the smallest dimension in the tapered perforations in the diamond anvils, and also smaller than the 250 μm diameter of the gasket hole that holds the sample. The incident flux on the DAC is $\sim 10^{11}$ photons/s for photon energies near 7 keV.

The nonmagnetic, copper-beryllium DAC model WCM-7B is manufactured by easyLab Technologies Ltd., previously Diacell. The DAC is in thermal contact with the cold finger of a Helitran He-flow cryostat manufactured by Advanced Research Systems. Silicon-diode thermometers on the cold finger and the outer wall of the CuBe cell show a small temperature gradient of $\lesssim 1$ K after equilibration. The cell reaches a typical base temperature of ~ 9 K. The cryostat is mounted on the high resolution *x*, *y*, *z* translation stages of a Huber motorized cryostat carrier. These are used for sample positioning in the x-ray beam with micron resolution. A coarse, long-travel *X*-translation stage allows motion of the cryostat in and out of the electromagnet, which is required for sample mounting. Furthermore, with transparent windows on the cryostat's vacuum shroud, this position allows for pressure calibration using conventional ruby fluorescence measurements. A Huber 410 goniometer holds the cryostat carrier and also allows for a θ rotation of the cryostat/DAC assembly about the vertical axis. This rotation is used to minimize unwanted Bragg diffraction from the single crystalline diamond anvils, which can introduce spurious glitches in the absorption spectra. The electromagnet is manufactured by GMW and features hollowed pole pieces with $\sim$3-mm-diameter holes for x-ray transmission. It reaches a maximum field of 7 kOe at a gap of 50 mm, the width of the vacuum shroud. Gas ionization chambers are used to monitor the incident and transmitted x-ray intensities. Accounting for sample, pressure medium, and pressure calibrant absorption, the typical x-ray flux transmitted through the DAC is $\sim 5 \times 10^8$ photons/s. The XMCD data are recorded in helicity-switching mode (12.7 Hz), and the related modulation in absorption coefficient is detected with a phase lock-in amplifier at each energy point through the absorption edge.[17] Helicity switching is achieved by a piezoelectric actuator, which rotates the C(111) diamond crystal away from the Bragg condition by the angular offset needed to attain the quarter wave-plate condition ($\pi/2$ phase shift between σ, π polarization components parallel and perpendicular to the Bragg diffraction plane). At 7 keV, this angular offset is $\sim$0.1 mrad for a 100-μm-thick diamond crystal.[16]

B. Diamond anvil cell

The pressure is changed *in situ* by controlling the He-gas pressure in an expanding membrane that drives piston motion, without the need to warmup the cryostat and remove the cell from the cold finger. The disadvantage of membrane-driven cells for XMCD measurements is their relatively large size compared to their screw-type counterparts, which limits the minimum gap between the pole pieces of the electromagnet and constrains the maximum attainable magnetic field. Similarly, it prevents insertion of the DAC in the bore of most superconducting cryostat magnets. The axial dimension of the DAC is $\sim$40 mm, including the gas inlet tube.

The DAC is shown in Fig. 2, which also includes a schematic of the asymmetric diamond anvil configuration used in our experiments. This configuration is similar to that reported by Dadashev *et al.* for Mössbauer spectroscopy experiments at 14.4 keV.[18] The asymmetric anvil configuration retains a smooth optical surface on the minianvil side, allowing for *ex situ* ruby fluorescence to be collected for pressure calibration. The inner surface of the conical partial perforation is rough and strongly scatters fluorescence light, reducing its intensity. The perforated diamond anvils are manufactured by D'anvils Ltd. Anvil perforations are tapered, from 1.0 to $\sim$0.1–0.15 mm, with the inner wall in the partially perforated anvil being $\sim$0.1–0.2 mm thick. The minianvil is 0.7 mm high, resulting in a total of $\lesssim$0.9 mm of diamond in

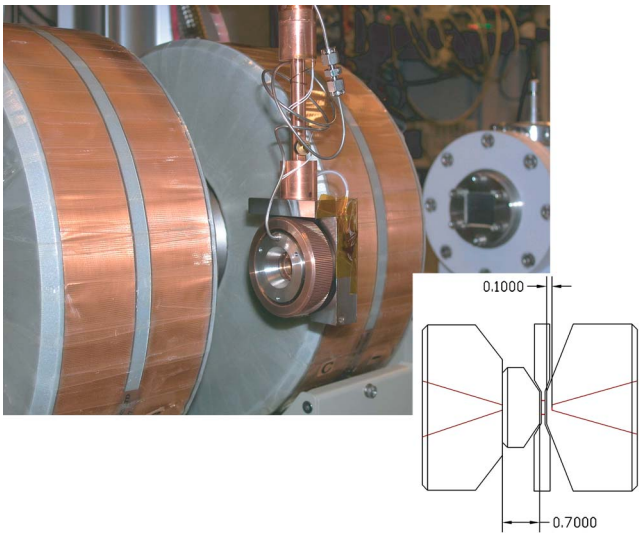

FIG. 2. (Color online) Membrane-driven diamond anvil cell mounted on the cold-finger extension of a He-flow cryostat (vacuum shroud not shown). A schematic of the asymmetric diamond anvil configuration featuring partially and fully perforated anvils is shown in the inset.

the x-ray path. Diamond culet size varies depending on the highest target pressure. So far culet sizes in the 450–600 μm range have been used to reach pressures of ~15–20 GPa.

C. Pressure calibration

Pressure is calibrated *in situ* using x-ray absorption fine structure measurements[19,20] on a pressure calibrant. Copper is a suitable calibrant as it has a cubic structure, a known compressibility,[21] and a Cu *K* absorption edge (8.979 keV) that is in relatively close proximity to the energy range of interest of most measurements. X-ray absorption fine structure (XAFS) measures the radial distribution function of atoms around the absorbing atom,[20] and hence it can determine pressure by comparing changes in bond length against the known compressibility curve of the calibrant. Figure 3(a) shows raw absorption data at the Cu *K* edge of a reference Cu powder sample. The fine Cu powders ($\lesssim 1$ μm) were carefully mixed with similarly fine powders of the sample of interest ($Gd_5Si_2Ge_2$) and thoroughly dispersed in the silicon-oil pressure medium before loading into the 250 μm hole of a nonmagnetic stainless steel gasket that had been preindented to 80 μm. The volume ratio was ≈1:1:15 for sample, calibrant, and pressure medium, respectively, in order to yield sample and calibrant absorptions of $\mu_{(s,c)}t_{(s,c)} \sim 1-2$, where μ is the absorption coefficient and t is the effective sample thickness. The inset in Fig. 3(a) shows the XAFS fine structure $\chi(k)=(\mu(k)-\mu_0(k))/\Delta\mu_0$ after background removal. Here k is the photoelectron wave number $k=\sqrt{2m(E-E_0)}/\hbar$, E_0 is the absorption threshold selected near the middle point of the rising absorption edge, μ_0 is a smoothly varying absorption background, and $\Delta\mu_0$ is its absorption edge jump. In a single scattering approximation the phase of the XAFS oscillations is related to the bond length R_i by $\chi(k) \sim \Sigma_i \sin(2kR_i+\delta_i)$, where the sum is over all bond lengths and δ_i are scattering phase shifts. A volume contraction results in a reduction of the photoelectron phase $2kR$ and

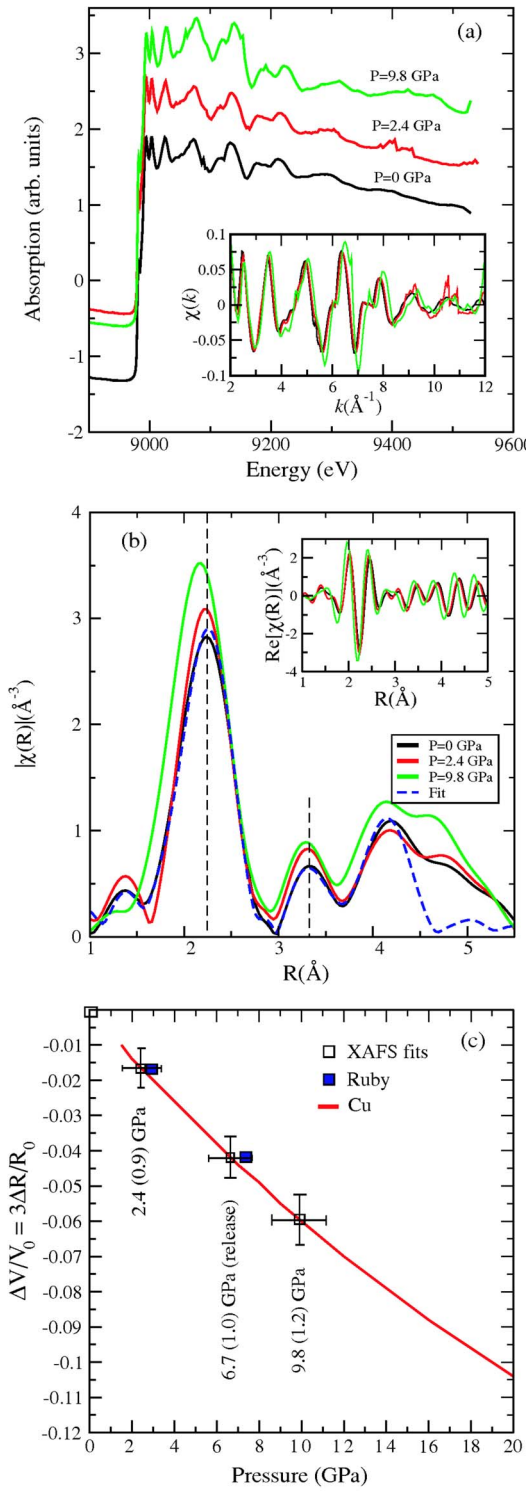

FIG. 3. (Color online) (a) Raw Cu *K*-edge absorption data at different pressures. The background-removed XAFS data are shown in the inset. (b) Magnitude (main panel) and real part (inset) of the complex Fourier transform of XAFS data, together with representative fits. (c) Pressure calibration using the volume reduction measured by XAFS (empty squares) and the compressibility of Cu at 300 K (red curve). Pressure calibration from ruby fluorescence is also shown (filled squares).

a related elongation of the *k*-dependent XAFS oscillations. The changes in interatomic distance with pressure are also clearly seen in the magnitude of the complex Fourier transform (FT) of the XAFS data shown in Fig. 3(b). In addition

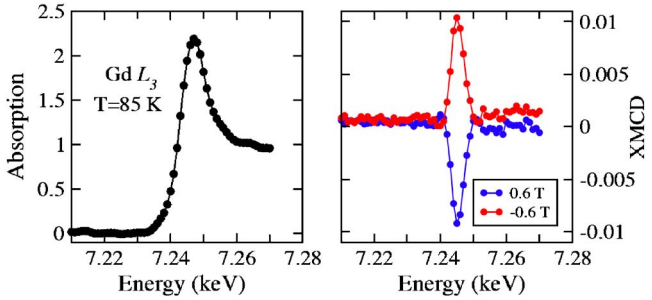

FIG. 4. (Color online) X-ray absorption (left) and x-ray magnetic circular dichroism (right) measurements at the Gd L_3 edge of $Gd_2Si_2Ge_2$ powders at an applied pressure of 2.4(0.9) GPa.

to a clear shift to shorter distances, an increase in XAFS amplitude is also evident. The latter is due to a decrease in bond-length vibrational disorder upon volume reduction.

The XAFS data are fitted in real space using FEFF6.0 theoretical standards.[22] The fits use data in the $k=[2,10]$ Å^{-1} range, assume a uniform compressibility of all Cu–Cu bonds and include contributions from the first three atomic shells around the Cu absorbing atom (triangular multiple scattering paths in the $R=1.8-4.5$ Å fitting range are also included). The pressure is obtained from the fitted volume change $\Delta V/V_0=3\Delta r/r_0$, where Δr is the change in bond length relative to its value at ambient pressure r_0, by interpolating into the known compressibility curve of Cu at 300 K.[21] This method yields an absolute accuracy of ~0.5–1 GPa, which is mostly determined by the precision of XAFS for average distance determination of ~0.002–0.005 Å. Relative pressure changes, however, can be determined with a much higher accuracy of ~0.1 GPa. Figure 3(c) compares the XAFS-derived pressures with those obtained with *ex situ* conventional ruby fluorescence for two sample conditions (after loading and after pressure release). The two methods agree within experimental errors.

III. TEST CASE: GIANT MAGNETOCALORIC MATERIAL $Gd_5Si_2Ge_2$

The high-pressure XMCD capability was tested on the giant magnetocaloric material $Gd_5(Si_xGe_{1-x})_4$ ($x=0.5$). This material has recently attracted much attention as a potential refrigerant material for applications in magnetic refrigeration near room temperature.[11,12] A first-order, martensiticlike magnetostructural phase transition yields a giant magnetocaloric effect where adiabatic temperature changes as high as 16 K can be obtained in the vicinity of room temperature through the application and removal of applied fields below about 5 T.[11] The magnetostructural transition is strongly affected by the Si content x. Silicon doping contracts the lattice and linearly enhances the transition temperature for $x \leqslant 0.5$, while the transition becomes purely magnetic with a lower rate of increase in transition temperature with doping for $x>0.5$.[11]

Figure 4 shows the Gd L_3 x-ray absorption data (left) and corresponding XMCD data (right) for a $Gd_5Si_2Ge_2$ sample at an applied pressure of 2.4(0.9) GPa. The pressure is determined from XAFS measurements on Cu powders loaded with the sample, as discussed in Sec. II C. The pressure medium was silicon-oil and the anvils' culet size was 600 μm. The XMCD data were measured in helicity-switching mode (12.7 Hz) using a phase lock-in detection scheme.[17] Hysteresis loops using a 4 T superconducting magnet show that the magnetization of the sample at the $H=0.6$ T applied field is reduced by a factor of 6 relative to its saturation value. The XMCD signal reverses sign upon field reversal, as expected.

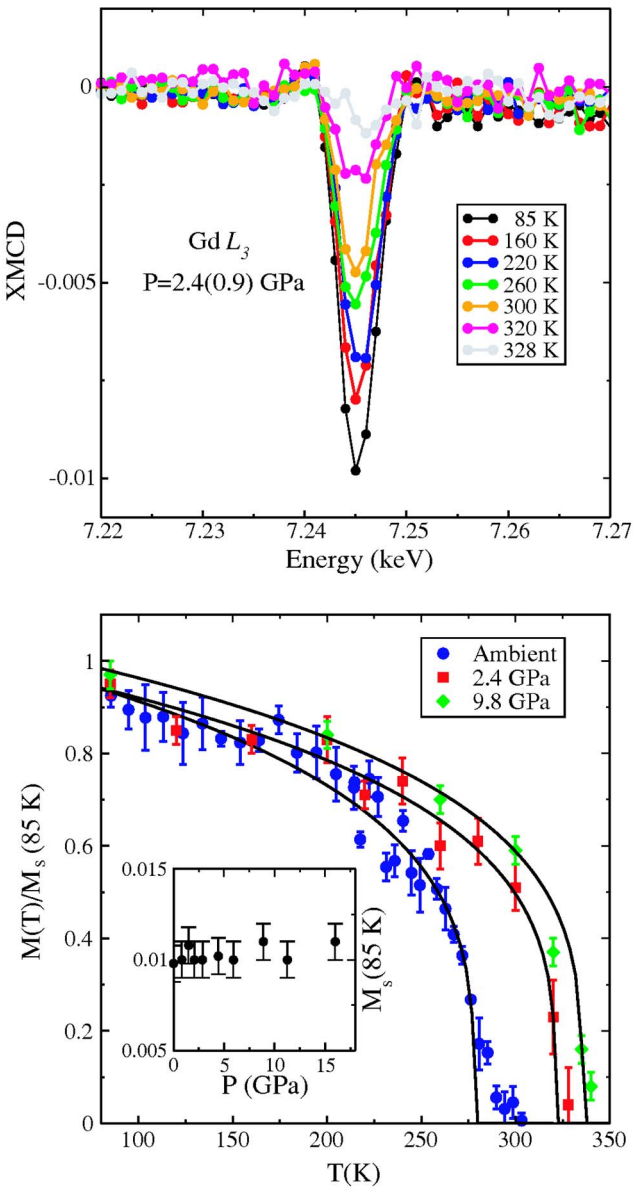

FIG. 5. (Color online) Top: Temperature-dependent Gd L_3-edge XMCD data at $P=2.4(0.9)$ GPa and $H=0.6$ T. Bottom: Pressure dependence of the magnetic transition at $H=0.6$ T. The inset shows saturation magnetization ($T=85$ K, $H=0.6$ T) as a function of applied pressure.

Figure 5 (top) shows the temperature-dependent XMCD data at $P=2.4(0.9)$ GPa, measured on warming. The magnetic transition temperature at this pressure is $T_c=321\pm6$ K, a 44 K enhancement relative to the $T_c=277\pm2$ K at ambient pressure (Fig. 5, bottom). As with Si doping, pressure induces a first-order monoclinic (M) to orthorhombic (O) transition in $Gd_5Si_2Ge_2$ within a pressure range of 1.0–2.0 GPa with a concomitant change in T_c from 275 to 305 K.[14,23]

Raising the pressure further or increasing the Si doping yields additional T_c increases, albeit at a lower rate.[13,14] Our smallest pressure of 2.4 GPa is enough to cause the $M \rightarrow O$ transition and yield a large T_c increase, while much smaller T_c increases are observed at higher pressures [$T_c = 336 \pm 4$ K at 9.8(1.2) GPa; see Fig. 5, bottom]. The rate of increase in T_c between 2.4 and 9.8 GPa is $dT_c/dP = 2.0 \pm 0.7$ K GPa^{-1}, similar to the 3.0 K GPa^{-1} reported for a $x = 0.8$ sample by Morellon *et al.*[13] but significantly smaller than the 9.0 K GPa^{-1} reported by Carvalho *et al.*[14] The saturation magnetization, also shown in Fig. 5, is nearly unchanged with increasing pressure up to ~16 GPa.

IV. SUMMARY

By combining a CuBe diamond anvil cell featuring perforated anvils and remote control of piston motion, a helium flow cryostat, and an electromagnet, we have developed an instrument that allows efficient collection of x-ray magnetic circular dichroism data at high pressures (~20 GPa), low temperatures (~9 K), and high fields (~7 kOe). Coupled with focusing optics and polarizing insertion devices or diffracting optics available at hard x-ray ($\gtrsim$5 keV) XMCD synchrotron beamlines, this capability offers unique opportunities to unravel the effects of pressure upon the magnetic properties of complex magnetic materials.

ACKNOWLEDGMENTS

Work at Argonne is supported by the U.S. Department of Energy, Office of Science, Office of Basic Energy Sciences, under Contract No. DE-AC-02-06CH11357. The authors would like to thank Dr. Valentin Iota whose earlier experiments at beamline 4-ID-D greatly impacted the development of this instrument. They also thank Dr. Ya. Mudryk, Dr. V. K. Pecharsky, and Dr. K. A. Gschneidner for providing the $Gd_5Si_2Ge_2$ powders.

[1] W. Heisenberg, Z. Phys. **49**, 619 (1928).
[2] P. W. Anderson, Phys. Rev. **79**, 350 (1950).
[3] M. A. Ruderman and C. Kittel, Phys. Rev. **96**, 99 (1954); T. Kasuya, Prog. Theor. Phys. **16**, 45 (1956); K. Yosida, Phys. Rev. **106**, 893 (1957).
[4] G. Schutz *et al.*, Phys. Rev. Lett. **58**, 737 (1987); P. Carra and M. Altarelli, *ibid.* **64**, 1286 (1990); J. Stohr, J. Magn. Magn. Mater. **200**, 470 (1997).
[5] O. Mathon, F. Baudelet, J.-P. Itié, S. Pasternak, A. Polia, and S. Pascarelli, J. Synchrotron Radiat. **11**, 423 (2004); E. Duman, M. Acet, E. F. Wassermann, J. P. Itié, F. Baudelet, O. Mathon, and S. Pascarelli, Phys. Rev. Lett. **94**, 075502 (2005).
[6] N. Ishimatsu *et al.*, Nucl. Instrum. Methods Phys. Res. A **467**, 1061 (2001); N. Ishimatsu *et al.*, J. Phys. Soc. Jpn. **72**, 2372 (2003).
[7] V. Iota, J.-H. Park Klepeis, C.-S. Yoo, J. Lang, D. Haskel, and G. Srajer, Appl. Phys. Lett. **90**, 042505 (2007).
[8] J. Goulon, A. Rogalev, F. Wilhelm, N. Jaouen, C. Goulon-Ginet, and C. Brouder, Eur. Phys. J. B **53**, 169 (2006).
[9] H. Maruyama, J. Synchrotron Radiat. **8**, 125 (2001).
[10] D. Haskel, J. C. Lang, Z. Islam, A. Cady, G. Srajer, M. van Veenendaal, and P. C. Canfield, Phys. Rev. Lett. **95**, 217207 (2005).
[11] V. K. Pecharsky and K. A. Gschneidner, Jr., Adv. Mater. (Weinheim, Ger.) **13**, 683 (2001).
[12] F.-J. Perez-Reche, F. Casanova, E. Vives, L. Manosa, A. Planes, J. Marcos, X. Batelle, and A. Labarta, Phys. Rev. B **73**, 014110 (2006).
[13] L. Morellon, Z. Arnold, P. A. Algarabel, C. Magen, M. R. Ibarra, and Y. Skorokhod, J. Phys.: Condens. Matter **16**, 1623 (2004).
[14] A. M. G. Carvalho, C. S. Alves, A. de Campos, A. A. Coelho, S. Gama, F. C. G. Gandra, P. J. van Ranke, and N. A. Oliveira, J. Appl. Phys. **97**, 10M320 (2005).
[15] J. W. Freeland, J. C. Lang, G. Srajer, R. Winarski, D. Shu, and D. M. Mills, Rev. Sci. Instrum. **73**, 1408 (2002)
[16] K. Hirano, K. Izumi, T. Ishikawa, S. Annaka, and S. Kikuta, Jpn. J. Appl. Phys., Part 2 **30**, L407 (1991); J. C. Lang and G. Srajer, Rev. Sci. Instrum. **66**, 1540 (1995).
[17] M. Suzuki, N. Kawamura, M. Mizumaki, A. Urata, H. Maruyama, S. Goto, and T. Ishikawa, Jpn. J. Appl. Phys., Part 2 **37**, L1488 (1998).
[18] A. Dadashev, M. P. Pasternak, G. Kh. Rozenberg, and R. D. Taylor, Rev. Sci. Instrum. **72**, 2633 (2001).
[19] S. Kelly, R. Ingalls, F. Wang, B. Ravel, and D. Haskel, Phys. Rev. B **57**, 7543 (1998).
[20] E. A. Stern, Phys. Rev. B **10**, 3027 (1974); P. A. Lee and J. B. Pendry, *ibid.* **11**, 2795 (1975).
[21] A. Dewaele, P. Loubeyre, and M. Mezouar, Phys. Rev. B **70**, 094112 (2004).
[22] S. I. Zabinsky, J. J. Rehr, A. Ankudinov, R. C. Albers, and M. J. Eller, Phys. Rev. B **52**, 2995 (1995).
[23] Ya. Mudryk, Y. Lee, T. Vogt, K. A. Gschneidner, Jr., and V. K. Pecharsky, Phys. Rev. B **71**, 174104 (2005).